Underwater acoustic MIMO OFDM: an experimental analysis

Underwater Acoustic MIMO OFDM: An Experimental Analysis

Guillem Palou
MIT Sea Grant College Program
Email: gpalou@mit.edu

Milica Stojanovic
Northeastern University
Email: millitsa@ece.neu.edu

***Abstract*—Performance of multiple-input multiple-output (MIMO) orthogonal frequency division multiplexing (OFDM) is analyzed on an experimental shallow water acoustic channel. Different modulation levels, numbers of subcarriers and transmitters were tested over a period of two weeks. The objectives in doing so were (a) to assess the effect of environmental conditions on the system performance, (b) to determine the performance limits and the data rate supported by the existing detection methods, and (c) to investigate the possibility to push these limits by employing methods for inter-carrier interference (ICI) compensation.**

I. Introduction

OFDM systems offer an attractive way of coping with the frequency selectivity of underwater acoustic (UWA) channels by dividing the overall bandwidth into a set of narrow-band channels, each characterized by flat fading. The advantage of OFDM lies in the simplicity of modulation / demodulation process, which is efficiently implemented by means of FFT.

Low speed of sound results not only in long multipath delay spreads underwater, but also in frequency-dependent Doppler shifts that arise due to intentional transmitter / receiver motion or their drifting with the currents and waves [1], [2]. Earlier work on UWA OFDM systems addressed several approaches for synchronization and data detection in the presence of Doppler distortion. In [1], a block-by-block approach is adopted, in which each OFDM block is detected independently. After initial resampling, carrier frequency offset is assumed to be equal for all the subcarriers, and compensation is performed accordingly. MIMO OFDM detection based on this synchronization method was considered in [3]. In [2], a method for non-uniform (frequency-dependent) Doppler compensation is proposed, which is implemented in an adaptive fashion to exploit temporal correlation between adjacent blocks. In [4] , this method is combined with sparse channel estimation, while [5], [6] and [7] extend the concept to MIMO OFDM detection.

In its simplest, conventional form, an OFDM system is designed under the assumption that the channel impulse response (CIR) is time-invariant over one block (one OFDM symbol). The block duration is thus a critical design parameter, which must be determined in accordance with the coherence time of the channel. Specifically, the block duration must be kept (well) below the coherence time of the channel; otherwise, the CIR may change significantly within a block, causing loss of carrier orthogonality and giving rise to inter-carrier interference (ICI). Hence, there is a trade-off in the selection of block duration for a given system: a shorter block ensures the absence of ICI and allows minimal-complexity conventional processing, but it results in a poor utilization of the system resources, since each block must be followed by a multipath guard time. One way to increase the system efficiency is by use of multiple, spatially multiplexed channels. Although the block duration is kept below the ICI limit, the receiver now has to deal with multiple (MIMO) channel estimation and cross-talk. Another possibility is to allow for an increased block duration (a greater number of subcarriers) and deal with the resulting ICI through more complex processing at the receiver.

Methods for ICI compensation have been extensively studied in the general communications literature, and performance bounds for radio channels have been established [8]. Specific algorithms for ICI compensation, e.g. [9] and [10], have been proposed, and different channel models have been used to asses the system performance. Reduced complexity algorithms that eliminate the need for large matrix inversion were addressed in [11]. In [12], [13], these inversions are performed using LDL factorization, while the algorithm [14] exploits a low-complexity model of the channel's time variation.

In comparison with the radio channels, the problem of ICI in acoustic channels has only recently come to the research forefront [15]. Recent contributions include [16] and [17], which focus on the problem of UWA ICI modeling and suppression.

The goal of our study is to assess the impact of the channel's time variation on the system performance in a realistic, experimental setting. In particular, we want to answer the following questions: 1) at which point is a performance limit reached when conventional detection methods are used, i.e. what is the limit on the number of transmitters and subcarriers in a given bandwidth; 2) does this limit depend on the environmental conditions such as wind, waves, etc., that cause the channel to vary in time, and 3) can this limit be pushed through the use of ICI compensation techniques.

The data used in this study were collected over the course of a two week experiment, conducted in October 2008 near the island of Martha's Vineyard off the coast of New England. Bottom-mounted transmitter / receiver arrays were deployed, operating in about 15 m of water at a 1 km range. Varying modulation parameters were tested in the 8-18 kHz band.

0-933957-38-1/09/$20.00

The paper is organized as follows. In Sec.II, OFDM system model is captured, and the experimental setting is described. In Sec.III, MIMO OFDM processing method [6] is summarized, and its performance on real data is discussed in light of varying environmental conditions, number of subcarriers and transmitters. Sec.IV addresses the problem of ICI, outlining the algorithms used, and the improvement they offered. Finally, conclusions are summarized in Sec.V.

II. System description

The transmitted signals were of the zero-padded OFDM type, given by

$$\begin{aligned} s(t) &= Re\{u(t)e^{j2\pi f_0 t}\} \\ u(t) &= \sum_{k=0}^{K-1} d_k(n)g(t-nT')e^{j2\pi k\Delta f(t-nT')} \end{aligned} \quad (1)$$

where $g(t)$ is a unit-amplitude rectangular pulse of duration T, $T' = T + T_g$ is the signaling interval that includes the multipath guard time T_g, f_0 is the lowest carrier frequency, $\Delta f = 1/T$ is the subcarrier spacing, K is the number of subcarriers, and $d_k(n)$ is the data symbol transmitted on the k-th subcarrier during the n-th signaling interval. In the case of multiple transmitters, a different data stream, $d_k^t(n)$, $t = 1, \dots M_T$, was used to modulate each of the M_T transmitted signals.

The experiment, called the Surface Processes Acoustic Communications Experiment (SPACE), was conducted in October 2008, south of the island of Martha's Vineyard off the coast of New England. Fig.1 illustrates the deployment geometry. The transmitter array (4 elements separated by 50 cm) and the receiver array (12 elements, separated by 12 cm) were fixed on the ocean floor.

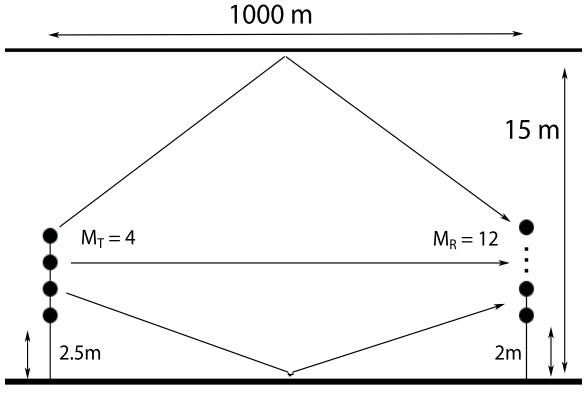

Fig. 1. Geometry of the experiment (southwest-southeast).

The signals were transmitted around the clock over the course of 15 days. The same group of signals, lasting two minutes, was repeated every two hours. Each such group contained several OFDM frames with varying modulation parameters. Table I lists the signal parameters.

bandwidth, B	10 kHz
lowest carrier frequency, f_0	8.25 kHz
sampling frequency, $f_s = 4B$	40 kHz
modulation method	QPSK, 8-PSK
coding	BCH (64,10)
symbols per frame, N_d	16384
number of carriers, K	128, 256, 512, 1024
carrier spacing, Δf [Hz]	78, 39, 19, 10
block duration, $T = 1/\Delta f$ [ms]	13, 26, 52, 105
blocks per frame, $N = N_d/K$	128, 64, 32, 16
guard time, T_g	16 ms

TABLE I
Signal parameters.

This selection of signal parameters corresponds to a large range of bandwidth efficiencies, 0.9-10.4 without coding, or 0.1-1.6 with a 1/6 rate code. Not counting the code rate, the bandwidth efficiency is defined as the ratio of the bit rate to the bandwidth occupied,

$$\frac{R_b}{B} = M_T\frac{mK}{T'} = M_T\frac{m}{1+T_gB/K} \quad (2)$$

where m is the number of bits per symbol, e.g. 3 if 8-PSK is used.

The conditions during the experiment were varying, with periods of high wave activity. Fig.2 shows the wind speed, wave height, and wave period observed during the experiment. As we will see in Sec.III, the system performance is related to some of these parameters; in particular, it appears to deteriorate during the periods of increased wave height. We conjecture that this behavior is caused by the fact that the CIR varies more rapidly during such periods.

III. Receiver performance

In this section, we focus on a MIMO OFDM detection algorithm proposed in [6]. This algorithm is based on a channel model that assumes the CIR to be fixed during one OFDM block, but allows it to change from one block to another. The signal after FFT demodulation can then be represented as

$$\mathbf{Y}(n) = \mathbf{\Delta}(n)\mathbf{h}(n) + \mathbf{Z}(n) \quad (3)$$

where the matrix $\mathbf{Y}(n)$ contains $K \times M_R$ signals received across K subbands and M_R elements, and $\mathbf{Z}(n)$ contains the corresponding noise components. The channel is modeled by the matrix

$$\mathbf{h}(n) = \begin{bmatrix} \mathbf{h}_{-A}(n) \\ \vdots \\ \mathbf{h}_{L-1-A}(n) \end{bmatrix} \quad (4)$$

where each component $\mathbf{h}_l(n)$ is an $M_T \times M_R$ matrix whose elements represent the l-th channel tap of a given transmitter/receiver pair. The total multipath span is L taps, and the indexing distinguishes A "anti-causal" taps. The $K \times M_T L$ matrix $\mathbf{\Delta}(n)$ captures the data symbols and the phase distortions, and it is given by

$$\mathbf{\Delta}(n) = [\mathbf{\Phi}^{-A}\mathbf{D}_\theta(n) \dots \mathbf{\Phi}^{L-1-A}\mathbf{D}_\theta(n)] \quad (5)$$

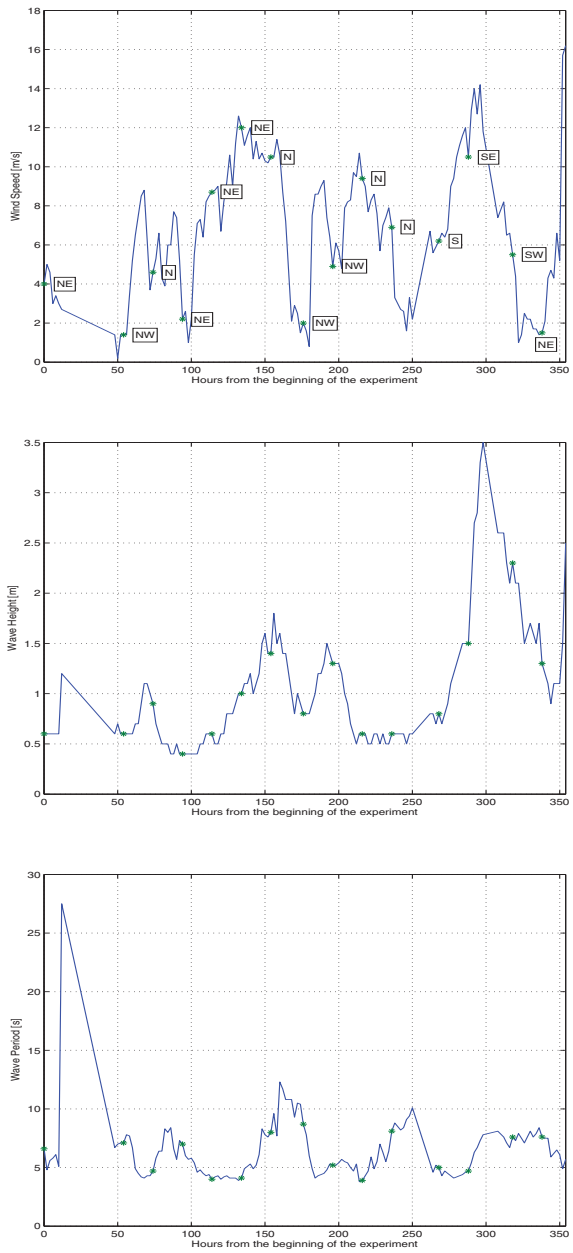

Fig. 2. Wind speed with wind direction indicated, wave height and wave period during the experiment. Stars mark the exact points in time when OFDM signals were recorded.

where $\mathbf{\Phi} = \text{diag}[e^{-j2\pi k/K}]_{k=0,\dots K-1}$, and $\mathbf{D}_\theta(n)$ is a $K \times M_T$ matrix with entries $d_k^t(n)e^{j\theta_k^t(n)}$, where $\theta_k^t(n)$ models the phase distortion between the t-th transmitter and the receiver array.

Based on this model, the channel is estimated as follows. Assuming that the data symbols are known for the first block ($n = 0$), the phases are set to zero, and the initial estimate is obtained as

$$\hat{\mathbf{h}}(0) = [\mathbf{\Delta}'(0)\mathbf{\Delta}(0)]^{-1}\mathbf{\Delta}'(0)\mathbf{Y}(0) \qquad (6)$$

where the prime denotes conjugate transpose. This estimate is used to judge the channel sparseness, i.e. to identify those J taps (matrices $\mathbf{h}_{l_1}(0), \dots \mathbf{h}_{l_J}(0)$) that contain entries whose magnitude is above some threshold. The remaining taps are then set to zero, as they do not contribute significantly to the CIR. The adaptation now proceeds according to one of two algorithms: the first requires a matrix inversion of size $M_T J \times M_T J$, while the second does not. For purposes of illustration, we will summarize the second algorithm.

The sparse system model follows directly from the expressions (3) - (5). The matrix $\mathbf{\Delta}(n)$ in these expressions simply needs to be substituted by a reduced-size, $K \times M_T J$ matrix $\underline{\mathbf{\Delta}}(n)$, which contains only the significant channel taps. The estimation algorithm is an adaptive algorithm of the least mean squares (LMS) type, which calculates the sparse channel estimate as

$$\hat{\underline{\mathbf{h}}}(n) = \hat{\underline{\mathbf{h}}}(n-1) + \mu\underline{\mathbf{\Delta}}'(n)[\mathbf{Y}(n) - \underline{\mathbf{\Delta}}(n)\hat{\underline{\mathbf{h}}}(n-1)] \qquad (7)$$

Further sparsing can now be performed by setting to zero those coefficients of $\hat{\underline{\mathbf{h}}}(n)$ whose magnitude is below the threshold. By doing so, the estimation noise is limited, resulting in an improved performance.

Once the channel estimates $\hat{\mathbf{h}}_l(n)$ are available, their discrete Fourier transform, $\hat{\mathbf{H}}_k(n)$, $k = 0, \dots, K-1$, is calculated via FFT, and used to perform data detection in the next block. Standard (zero-forcing) detection is employed, yielding the estimates of the M_T data symbols transmitted on the k-th subcarrier as

$$\hat{\mathbf{d}}_k(n) = \mathbf{y}_k(n)\hat{\mathbf{H}}'_k(n)[\hat{\mathbf{H}}_k(n)\hat{\mathbf{H}}'_k(n)]^{-1}\hat{\mathbf{\Theta}}^*_k(n) \qquad (8)$$

where $\mathbf{y}_k(n)$ is the k-th row of $\mathbf{Y}(n)$, and $\hat{\mathbf{\Theta}}_k(n) = \text{diag}[e^{j\hat{\theta}_k^1(n)} \dots e^{j\hat{\theta}_k^{M_T}(n)}]$ contains the phase estimates.[1] Decisions made on the data symbol estimates are now used to update the channel estimate, and so forth. The algorithm operates in a decision directed manner, and hence has minimal overhead (first block is reserved for training).

This algorithm was applied to the experimental data, to assess the performance in changing environmental conditions and derive general rules for the selection of system parameters. In particular, our goal was to identify the greatest number of carriers and transmit elements (greatest bandwidth efficiency) for which the performance meets some requirements.

Fig.3 shows an example of a channel response recorded during the experiment. Typically, the delay spread was below 10 ms, and $L = 128$ taps were chosen to capture the CIR (this corresponds to $128/B = 13$ ms). The algorithm was initiated using this value, and further sparsing was performed on-line. Depending on the time of transmission, the average number of channel coefficients kept was between 60 and 120. The channel tracking parameter μ was tuned once for each (M_T, K) configuration, and kept the same throughout the experiment. No pilot carriers were used.

[1] Phase tracking is based on Doppler factor prediction [2], and is crucial to the entire operation.

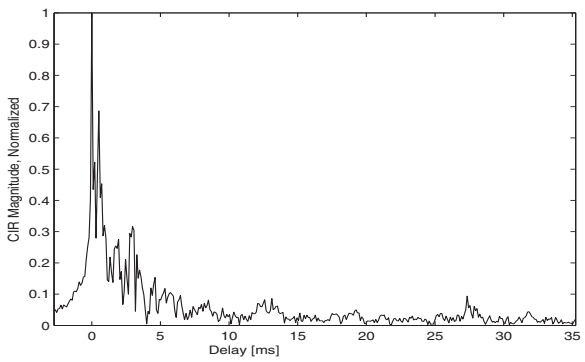

Fig. 3. A typical channel impulse response.

Receiver performance is summarized in Figs.4 and 5, which show the MSE and the BER for varying modulation parameters observed over the course of the experiment. The overall MSE is defined as an average taken over all the transmitters, subcarriers, and blocks,

$$MSE = \frac{1}{NKM_T} \sum_{n=0}^{N-1} \sum_{k=0}^{K-1} \sum_{t=1}^{M_T} |d_k^t(n) - \widehat{d}_k^t(n)|^2 \quad (9)$$

Focusing on the results for $M_T = 1$, we note that both modulation methods perform well. The performance degrades slightly as the number of carriers increases from 128 to 1024. This indicates that the performance is influenced by the time variability of the channel, but not limited by it. The uncoded BER varies following the same pattern as the MSE, but the coded BER stays at zero throughout the measurements.

As the number of transmit elements increases, the performance deteriorates, since the same physical channel is now used to transmit multiple data streams, which generate cross-talk. With M_T=2, the deterioration is gradual, and the system manages to separate multiple channels. It is interesting to note that lower values of K experience higher loss, thus reversing the performance trend with K. The exact way in which this effect takes place is rather hard to judge, because there exists an inherent trade-off between the number of carriers K and the system performance. On the one hand, a greater K implies a longer block, and, hence, a more substantial channel variation that can hurt the system performance (by creating ICI); on the other hand, a greater K provides more observations for the decision-directed channel estimator, thus boosting its performance.

From the viewpoint of bandwidth efficiency, it is of course advantageous to use the greatest possible number of subcarriers, and for the present experiment, we see that K=1024 is a good choice with M_T=2. Hence, this is a "win-win" situation, in which the bit rate is doubled by spatial multiplexing, while a large number of carriers provides efficient use of the multipath guard time without much compromise to the time-invariance assumption.

As M_T increases further, performance is lost in many instances. With M_T=3, lower values of K are the first to experience a complete loss in performance, while the system with more carriers copes with the changing conditions, showing periods of varying performance that coincide with those observed at M_T=1 and 2. At M_T=4, the system fails.

Performance loss with increasing M_T is inevitable, as the task of MIMO channel estimation becomes increasingly difficult in the presence of increased cross-talk between the channels. In fact, MIMO channel estimation is conditioned on having the number of transmitters $M_T \leq K/L$, which ensures the existence of the estimate (6). Hence, as more transmitters are added, this condition eventually becomes violated specially with lower values of K.

The limit on the number of transmitters implies a limit on the bandwidth efficiency (2):

$$\frac{R}{B} \leq \frac{K^2}{LK + L^2} \text{ [symbols/sec/Hz]} \quad (10)$$

Hence, for a given multipath spread L, which is proportional to BT_g, bandwidth efficiency is ultimately limited by the number of carriers. Although the time variability of the channel prevents the use of an arbitrarily large K, it is interesting to note that if one could use $K >> L$ without violating the time-invariance assumption, the bandwidth efficiency of the present implementation would be on the order of K/L symbols/second/Hz. Time variation, however, has to be taken into account, and if one were to offer a rule of thumb for the maximal number of transmitters, for the processing scheme used this could be $M_T < \beta K/BT_g$, where $\beta < 1$ is an environmental factor whose value should be decreased as the conditions worsen.

Variation in performance over the course of the experiment is quite obvious, and can be as large as several dB from one day to another, or even within a day. This naturally raises the question of performance dependence on the environmental conditions, such as wind and waves. For easy comparison, Fig.6 shows together the wave height and the MSE for the SIMO case. Clearly, there exists a correlation between the two, with increased MSE during the periods of high waves (which are in turn correlated with high wind speeds). A similar comparison with the wave period indicates a lower degree of correlation, but seems to link high values of MSE with short wave periods. This is an intuitively justifiable observation, since higher frequency of the waves implies a faster varying channel.

IV. ICI COMPENSATION

Based on our discussion so far, it is apparent that the quest for high transmission rates over band-limited acoustic channels is tightly coupled with the use of a large number of carriers K. Because this implies a greater channel variation over one OFDM block, in order to push the performance limits it becomes necessary to deal with the resulting ICI. To do so, we investigate linear methods for ICI compensation.

Focusing on the SISO case, let us denote by $x_k(n)$ the input to the ICI processor, corresponding to the k-th subcarrier and n-th OFDM block. This signal can be taken directly

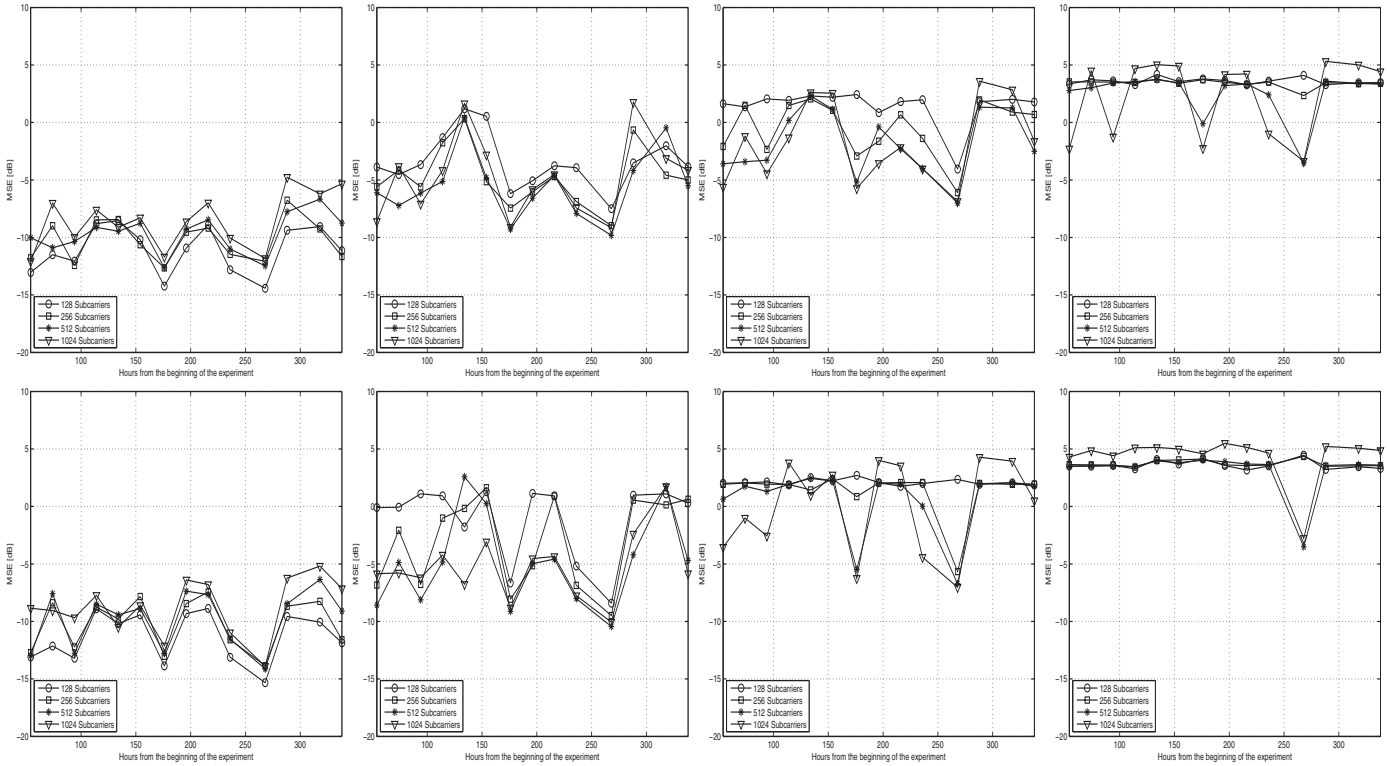

Fig. 4. MSE for QPSK (top) and 8-PSK (bottom) for varying number of transmitters, M_T=1, 2, 3 and 4 from left to right.

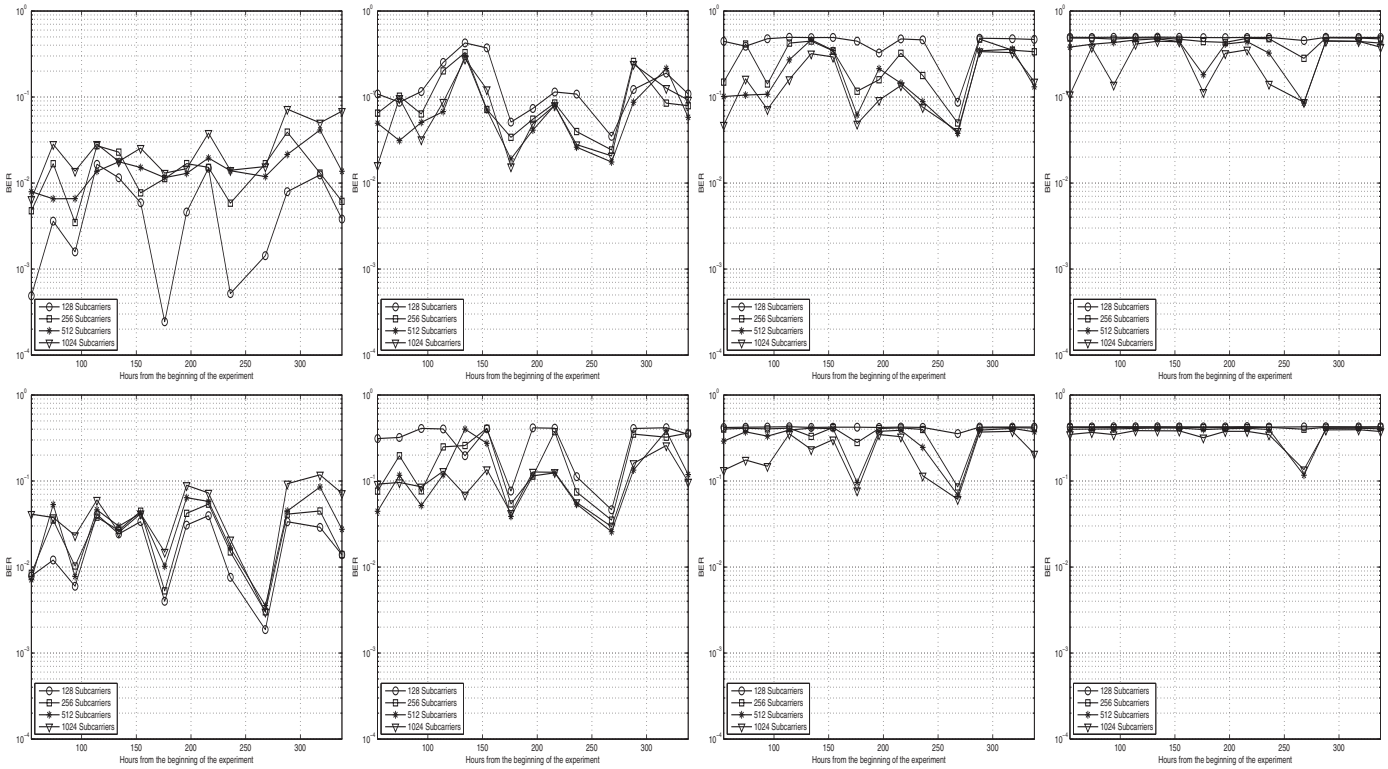

Fig. 5. BER without coding for QPSK (top) and 8-PSK (bottom) for varying number of transmitters, M_T=1, 2, 3 and 4 from left to right.

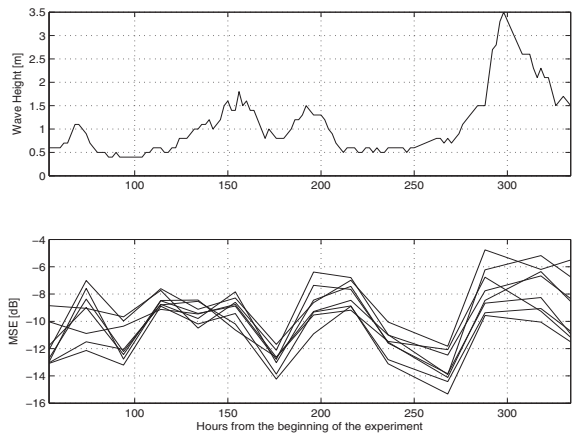

Fig. 6. Wave height and MSE (single transmitter, QPSK and 8-PSK with K=128, 256, 512, 1024 carriers).

from the FFT demodulator after phase compensation, $x_k(n) = y_k(n)e^{-j\hat{\theta}_k(n)}$.

In the SIMO case, the phase-corrected FFT outputs of each receiving element, $x_k^r(n)$, $r = 0, \dots M_R$, are first fed to an ICI processor associated with that element, yielding K outputs. The outputs corresponding to the same carrier are then combined across all M_R receivers to yield the final data symbol estimate. The combiner weights should ideally be optimized jointly with those of the ICI processor, but for the moment we restrict out attention to the SISO problem.

The signal $x_k(n)$ at the input to the ICI processor is modeled as

$$x_k(n) = \sum_{l=0}^{K-1} H_{k,l}(n)d_l(n) + w_k(n) \tag{11}$$

where $H_{k,l}(n)$ are the channel coefficients that describe the interference between carriers k and l, and $w_k(n)$ is the noise. The frequency-domain channel coefficients $H_{k,l}(n)$ can also be related to the time-domain coefficients $h_{p,q}(n)$ via the following transformation:

$$H_{k,l}(n) = \frac{1}{N_s}\sum_{p=0}^{L-1}\sum_{q=0}^{N_s-1} h_{p,q}(n)e^{j2\pi\frac{q(l-k)-lp}{N_s}} \tag{12}$$

The physical meaning of a time-domain coefficient $h_{p,q}(n)$ is that of the p-th tap of the overall discrete-time CIR observed at time $nT' + qT_s$, where $T_s = T/N_s$ is the sampling interval.

ICI suppression methods can be classified according to the structure of the processor (linear, decision-feedback equalizer), the way in which the equalizer coefficients are computed (directly, or indirectly from a CIR estimate), and the type of algorithm used for computation.

We focus on a method based on indirect calculation, in which the channel coefficients are determined first, and then used to calculate the equalizer filters. We use here the word "equalizer" for the ICI processor, since the problem of ICI mitigation in an OFDM system is analogous to the problem of intersymbol interference (ISI) equalization in a single-carrier system. We will reserve the word "adaptive" to signify adaptation between OFDM blocks, and use the word "recursive" to describe operations across subcarriers in a given block.

A. ICI equalization, SISO case

Different methods have been proposed in the literature to estimate the ICI coefficients $H_{k,l}(n)$. For example, the method proposed in [17] capitalizes on the fact that ICI is limited to nearby carriers, which simplifies the modeling equation (11) to

$$\begin{aligned} x_k(n) &= \sum_{i=-I}^{I} H_{k,k+i}(n)d_{k+i}(n) + w_k(n) \\ &= \mathbf{g}'_k(n)\underline{\mathbf{d}}_k(n) + w_k(n) \end{aligned} \tag{13}$$

where $\mathbf{g}'_k(n) = [H_{k,k+I}(n) \dots H_{k,k-I}(n)]$ and $\underline{\mathbf{d}}_k(n) = [d_{k+I}(n) \dots d_{k-I}(n)]^T$. Assuming that the channel vector $\mathbf{g}_k(n)$ changes slowly with the subcarrier index k, the channel estimator can be implemented as a recursive filter with coefficients $\hat{\mathbf{g}}_k(n)$. The input to the filter is the data sequence, and the output is an estimate $\hat{x}_k(n) = \hat{\mathbf{g}}'_k(n)\underline{\mathbf{d}}_k(n)$. The filter coefficients are calculated using a recursive algorithm, such as LMS or RLS, so as to minimize the estimation error $\epsilon_k(n) = x_k(n) - \hat{x}_k(n)$ in the mean square sense. Direct equalization, which was also treated in [17], is based on a similar recursion that now targets the equalizer filter directly.

The data symbols that are needed to perform channel estimation can be obtained as tentative decisions made using the classical approach, i.e. one that neglects the ICI. Alternatively, or in addition to tentative decisions, some carriers can be reserved for pilots.

Once the channel vectors are available, they are arranged into a matrix $\hat{\mathbf{H}}(n) = [\hat{H}_{k,l}(n)]_{k,l=0,\dots K-1}$, and the block of data symbols is estimated in the least squares (LS) fashion as

$$\hat{\mathbf{d}}(n) = [\hat{\mathbf{H}}'(n)\hat{\mathbf{H}}(n)]^{-1}\hat{\mathbf{H}}'(n)\mathbf{x}(n) \tag{14}$$

where $\mathbf{x}(n)$ is the column vector of observations $x_k(n)$. Note that since $\hat{\mathbf{H}}(n)$ is a $K \times K$ banded matrix with only $2I+1$ diagonals, the required inverse can be simplified, e.g. through LDL factorization [13].

A different method for ICI coefficient estimation has been proposed in [14]. This method is based on explicit modeling of the channel's time variation. Specifically, it employs a Taylor series expansion of the CIR coefficients, in which only the linear term is retained. Referring to the expression (12), the time-domain coefficients are modeled as

$$h_{p,q}(n) = h_p(n) + q \cdot \Delta h_p(n) \tag{15}$$

Assuming that the quantities $h_p(n)$ and $\Delta h_p(n)$ are known (they will be estimated later), the above relationship can be used in the expression (12) to obtain the frequency-domain channel coefficients $H_{k,l}(n)$. Specifically, we have that

$$H_{k,l}(n) = \delta_{k,l}\sum_{p=0}^{L-1} h_p(n)e^{-j2\pi\frac{lp}{N_s}} + \xi_{k,l}\sum_{p=0}^{L-1}\Delta h_p(n)e^{-j2\pi\frac{lp}{N_s}} \tag{16}$$

where $\delta_{k,l}$ is the Kronecker delta, and

$$\xi_{k,l} = \frac{1}{N_s} \sum_{q=0}^{N_s-1} q e^{j2\pi \frac{q(l-k)}{N_s}} \tag{17}$$

The channel coefficient $H_{k,l}(n)$ is thus expressed as a sum of two terms, one that represents the transfer function of the channel evaluated at the k-th carrier frequency at the beginning of the n-th block, and another that represents distortion due to ICI. Note that evaluation of the latter requires only one additional FFT, since the factors $\xi_{k,l}$ can be pre-computed.

The remaining question is that of estimating the coefficients $h_p(n)$ and $\Delta h_p(n)$, which represent the CIR at the beginning of a block, and its gradient. In [14], this task is accomplished using dedicated channel probes, which are periodically inserted between the OFDM blocks. Here, we propose a different approach that does not require the extra overhead. Namely, to obtain a fixed per-block CIR estimate $\hat{h}_p(n)$, we use the adaptive algorithm [2]. Once the CIR for the current (and the previous) block is known, the gradient is estimated as

$$\Delta\hat{h}_p(n) = \frac{\hat{h}_p(n) - \hat{h}_p(n-1)}{N_s'} \tag{18}$$

where $N_s' = T'/T_s$ is the number of samples corresponding to T', the time interval between two CIR estimates. Other estimation methods are of course possible (e.g., all the previous blocks could be exploited to obtain a smoother estimate of the gradient).

Once the frequency-domain channel coefficients have been computed, ICI equalization can proceed as before. The channel matrix $\hat{\mathbf{H}}(n)$ is built using a desired number of pre- and post-cursors I, and the data symbols are estimated according to the expression (14).

B. Multichannel combining

In a multichannel (SIMO) receiver, an ICI equalizer is associated with each receiving element. The equalizer corresponding to the r-th receiving element utilizes channel coefficients $\hat{H}^r_{k,l}(n)$, resulting in a set of (preliminary) data symbol estimates, $\hat{d}^r_k(n)$, one for each receiving element $r = 1, \ldots M_R$. The data estimates are obtained as before, according to the expression (14), after which they are combined to yield the final estimate

$$\hat{d}_k(n) = \sum_{r=1}^{M_R} c^r_k(n) \hat{d}^r_k(n) \tag{19}$$

where $c^r_k(n)$ are the combiner weights.

Assuming that the channel estimates are correct, we have that $\hat{d}^r_k(n) = d_k(n) + \nu_k(n)$, where $\nu^r_k(n)$ is the noise. This noise is correlated, both across the carriers and across the receiving elements. The combiner ignores the former in favor of computational complexity, but the latter can be accounted for via maximum ratio combining (MRC). However, to do so, one would need to know the variance of the input noise $w^r_k(n)$. A simpler approach is to perform equal-gain combining (EGC), i.e. to set the combiner weights to $c^r_k(n) = 1$.

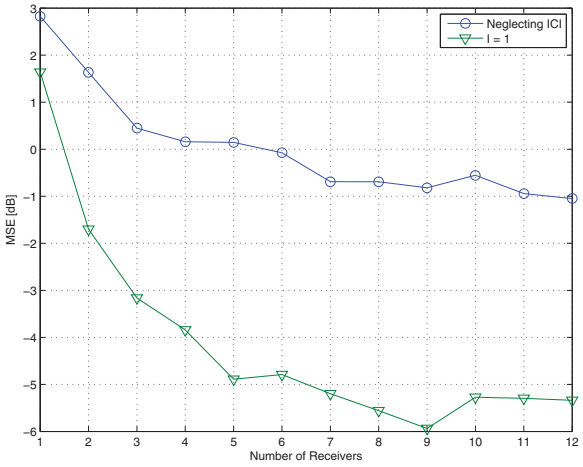

Fig. 7. Performance of ICI equalization and equal gain combining.

Although it may seem that combining and equalization are decoupled in this simple approach, we note that tentative symbol decisions used for ICI coefficient estimation are the ones obtained *after* combining; hence, there is a feedback by which the multichannel gain contributes to reliability.

Equal gain combining was coupled with ICI equalization and channel estimation via the Taylor series approximation. Fig7 illustrates the performance of this method on an experimental data set. We focus on the case with the largest number of carriers, K=1024, and one of the poor-quality recordings (hour 154) since this is where the effect of time-variation is most detrimental. Shown in the figure is the MSE (average over all the carriers in one block) vs. the number of receiving elements M_R. When fewer than 12 receivers are used, they are chosen to be maximally separated. The number of ICI coefficients used for equalization was 3 (I=1). The first block is reserved for initializing the channel estimator, and no pilots are used thereafter, i.e. the algorithm operates in a decision-directed mode. As a reference, the MSE of a receiver which neglects the ICI is included.

ICI equalization obviously offers a significant additional gain. The gain is evident even in the SISO case (M_R=1), although it is modest for the poor-quality data set at hand. As the number of receivers increases, so does the gain of the multichannel equalizer. With 2, 3, and 4 receivers, ICI equalization gains additional 3, 4 and 6 dB, approximately. By increasing the number of receivers beyond 5, the performance saturates with a gain of about 7 dB. Compared with the ICI-neglecting MRC [2], this is a gain of about 1 dB. The absolute level of the MSE is also worth noting. This level is directly correlated with the BER performance, and it needs to be above a certain threshold in order for the receiver to operate in a decision-directed mode. While the BER attained at an MSE of -1 dB is often insufficient, an MSE of -5 dB is certainly low enough to provide an open eye for the decoder.

V. Conclusion

An experimental analysis was conducted to assess the performance and establish the limits of OFDM, which is considered as a low-complexity solution for achieving high-rate communications over band-limited acoustic channels. Two parameters that are key to achieving high bandwidth efficiency in an OFDM system– the number of transmit elements M_T and the number of subcarriers K–were the focal point of experimentation, which included signal processing using (a) MIMO system configurations to support spatial multiplexing of M_T parallel data streams, and (b) ICI equalization to support an increase in K beyond the limit where the time-variation of the channel can be neglected.

Experimental results, obtained with signals recorded in shallow water over the course of two weeks, show variation in performance that can be correlated with the weather conditions, in particular with the wave height. The data set at hand demonstrates the possibility to use two transmit elements, thus doubling the bit rate, while using the largest number of carriers, K=1024. This "win-win" situation owes to decision-directed adaptive channel estimation and sparsing. Further increase in M_T leads to loss in performance.

The possibility to use large values of K rests on the system's ability to cope with the ICI. Experimental signals were processed using linear equalization in the frequency domain, with equalizer weights calculated from the ICI coefficients. The ICI coefficients were obtained using an adaptive channel estimator coupled with a linear model of the underlying time-variation. In a multichannel form, ICI equalization was shown to offer performance gains using simple equal gain combining. These preliminary results indicate that a careful receiver design, which respects the underlying physical processes, can be used to push the limits on the data rates that can be sustained over time-varying, band-limited acoustic channels. Future research should concentrate on new techniques for ICI equalization, as well as on coupling ICI equalization with MIMO detection.

Acknowledgment

This work was supported by the ONR MURI Grant #N00014-07-1-0738 and the ONR grant N00014-07-1-0202.

References

[1] B. Li, S. Zhou, M. Stojanovic, L. Freitag, and P. Willett, "Multicarrier communication over underwater acoustic channels with nonuniform Doppler shifts," *Oceanic Engineering, IEEE Journal of*, vol. 33, no. 2, pp. 198–209, April 2008.

[2] M. Stojanovic, "Low complexity OFDM detector for underwater acoustic channels," *OCEANS 2006*, pp. 1–6, Sept. 2006.

[3] B. Li, J. Huang, S. Zhou, K. Ball, M. Stojanovic, L. Freitag, and P. Willett, "Further results on high-rate MIMO-OFDM underwater acoustic communications," in *OCEANS 2008*, Sept. 2008, pp. 1–6.

[4] M. Stojanovic, "OFDM for underwater acoustic communications: Adaptive synchronization and sparse channel estimation," *Acoustics, Speech and Signal Processing, 2008. ICASSP 2008. IEEE International Conference on*, pp. 5288–5291, 31 2008-April 4 2008.

[5] S. Roy, T. Duman, and V. McDonald, "Error rate improvement in underwater MIMO communications using sparse partial response equalization," *OCEANS 2006*, pp. 1–6, Sept. 2006.

[6] M. Stojanovic, "Adaptive channel estimation for underwater acoustic MIMO OFDM systems," *Digital Signal Processing Workshop and 5th IEEE Signal Processing Education Workshop, 2009. DSP/SPE 2009. IEEE 13th*, pp. 132–137, Jan. 2009.

[7] P.C.Ceballos and M.Stojanovic, "Adaptive MIMO detection of OFDM signals in an underwater acoustic channel," *Proc. IEEE Oceans'08 Conference, Quebec City, Canada*, September 2008.

[8] X. Cai and G. Giannakis, "Bounding performance and suppressing intercarrier interference in wireless mobile OFDM," *Communications, IEEE Transactions on*, vol. 51, no. 12, pp. 2047–2056, Dec. 2003.

[9] T. Wang, J. Proakis, and J. Zeidler, "Techniques for suppression of intercarrier interference in OFDM systems," *Wireless Communications and Networking Conference, 2005 IEEE*, vol. 1, pp. 39–44 Vol. 1, March 2005.

[10] A. Gorokhov and J.-P. Linnartz, "Robust OFDM receivers for dispersive time varying channels: equalisation and channel acquisition," *Communications, 2002. ICC 2002. IEEE International Conference on*, vol. 1, pp. 470–474, 2002.

[11] X. Huang and H.-C. Wu, "Robust and efficient intercarrier interference mitigation for OFDM systems in time-varying fading channels," *Vehicular Technology, IEEE Transactions on*, vol. 56, no. 5, pp. 2517–2528, Sept. 2007.

[12] L. Rugini, P. Banelli, and G. Leus, "Simple equalization of time-varying channels for OFDM," *Communications Letters, IEEE*, vol. 9, no. 7, pp. 619–621, July 2005.

[13] L. Rugini, P.Banelli, and G.Leus, "Low-complexity banded equalizers for OFDM systems in Doppler spread channels," *EURASIP J. Appl. Signal Process.*, vol. 2006, pp. 248–248, January.

[14] G. Li, H. Yang, L. Cai, and L. Gui, "A low-complexity equalization technique for OFDM system in time-variant multipath channels," *Vehicular Technology Conference, 2003. VTC 2003-Fall. 2003 IEEE 58th*, vol. 4, pp. 2466–2470 Vol.4, Oct. 2003.

[15] I. Capoglu, Y. Li, and A. Swami, "Effect of doppler spread in ofdm-based uwb systems," *Wireless Communications, IEEE Transactions on*, vol. 4, no. 5, pp. 2559–2567, Sept. 2005.

[16] S. Mason, C. Berger, S. Zhou, K. Ball, L. Freitag, and P. Willett, "An OFDM design for underwater acoustic channels with Doppler spread," in *Digital Signal Processing Workshop and 5th IEEE Signal Processing Education Workshop, 2009. DSP/SPE 2009. IEEE 13th*, Jan. 2009, pp. 138–143.

[17] K. Tu, D. Fertonani, T. M. Duman, and P. Hursky, "Mitigation of intercarrier interference in OFDM systems over underwater acoustic channels," *IEEE Oceans 2009, Bremen, Germany*, May 2009.